The *drs* Tumor Suppressor Regulates Glucose Metabolism via Lactate Dehydrogenase-B

Yukihiro Tambe,[1] Masahiro Hasebe,[1,2] Chul Jang Kim,[3] Akitsugu Yamamoto,[2] and Hirokazu Inoue[1]*

[1]*Division of Microbiology and Infectious Diseases, Department of Pathology, Shiga University of Medical Science, Otsu, Shiga, Japan*
[2]*Department of Cell Biology and Bioscience, Nagahama Institute of Bioscience and Technology, Nagahama, Shiga, Japan*
[3]*Department of Urology, Kohka Public Hospital, Kohka, Shiga, Japan*

Previously, we showed that *drs* contributes to suppression of malignant tumor formation in *drs*-knockout (KO) mice. In this study, we demonstrate the regulation of glucose metabolism by *drs* using comparisons of *drs*-KO and wild-type (WT) mouse embryonic fibroblasts (MEFs). Extracellular acidification, lactate concentration, and glucose consumption in *drs*-KO cells were significantly greater than those in WT cells. Metabolomic analyses also confirmed enhanced glycolysis in *drs*-KO cells. Among glycolysis-regulating proteins, expression of lactate dehydrogenase (LDH)-B was upregulated at the post-transcriptional level in *drs*-KO cells and increased LDH-B expression, LDH activity, and acidification of culture medium in *drs*-KO cells were suppressed by retroviral rescue of *drs*, indicating that LDH-B plays a critical role for glycolysis regulation mediated by *drs*. In WT cells transformed by activated *K-ras*, expression of endogenous *drs* mRNA was markedly suppressed and LDH-B expression was increased. In human cancer cell lines with low *drs* expression, LDH-B expression was increased. Database analyses also showed the correlation between downregulation of *drs* and upregulation of LDH-B in human colorectal cancer and lung adenocarcinoma tissues. Furthermore, an LDH inhibitor suppressed anchorage-independent growth of human cancer cells and MEF cells transformed by activated *K-ras*. These results indicate that *drs* regulates glucose metabolism via LDH-B. Downregulating *drs* may contribute to the Warburg effect, which is closely associated with malignant progression of cancer cells.

Key words: *drs*; Warburg effect; lactate dehydrogenase; knockout mouse

INTRODUCTION

drs (down-regulated by v-*src)* was originally isolated as a transformation suppressor of the v-*src* oncogene [1,2], and *drs* mRNA expression is markedly downregulated in a variety of human cancer cell lines and malignant tumor tissues [3–9]. Moreover, malignant tumors, including lymphomas, lung adenocarcinomas, and hepatomas were generated in approximately 30% of *drs*-knockout (KO) mice [10], indicating that *drs* contributes to the suppression of malignant tumor formation. In our previous study, we demonstrated that *drs* is involved in apoptosis [11] and autophagy [12] under environmental stress conditions such as tumor formation and low serum culture. Ectopic expression of Drs induces apoptosis in human cancer cell lines via a novel pathway initiated from the endoplasmic reticulum (ER) by binding to ASY/Nogo-B/RTN-X_S and apoptosis-inducing proteins of ER, and activation of caspases 12, 9, and 3 [11]. In addition, *drs* regulates autophagic maturation induced by low serum stress by binding to the Rab GTPase protein, Rab24, which plays a role in autophagy [12]. These findings suggest that *drs* is involved in the determination of cell fate under environmental stress and plays protective roles against malignant tumor formation. Previously, we demonstrated the involvement of *drs* in host defense against a viral infection [13]. In the *drs*-KO MEFs infected with the vesicular stomatitis virus, viral protein synthesis and replication were markedly enhanced without upregulation of cellular protein

Abbreviations: BSA, bovine serum albumin; CE-ESI-TOFMS, capillary electrophoresis electrospray ionization time-of-flight mass spectrometr; CE-TOFMS, capillary electrophoresis time-of-flight mass spectrometry; DMEM, Dulbecco's modified eagle's medium; ER, endoplasmic Reticulum; ECAR, extracellular acidification rates; FBS, fetal bovine serum; GAPDH, glyceraldehyde-3-phosphate dehydrogenase; KO, knockout; LDH-A, lactate dehydrogenase-A; LDH-B, lactate dehydrogenase-B; MEF, mouse embryonic fibroblasts; MT, migration times; mTOR, mammalian target of rapamycin; OCR, oxygen consumption rates; PDK, pyruvate dehydrogenase kinases; PFK-M, phosphofructokinase-M; PKM2, pyruvate kinase M2; PPP, pentose phosphate pathway; qRT-PCR, quantitative reverse transcriptase-polymerase chain reaction; RIPA, radioimmunoprecipitation assay; RT-PCR, reverse transcriptase-polymerase chain reaction; SDS-PAGE, sodium dodecyl sulfate-polyacrylamide gel electrophoresis; TBS-T, Tris-buffered saline with Tween 20; TIGAR, TP53-inducible glycolysis and apoptosis regulator; WT, wild-type.

Grant sponsor: JSPS KAKENHI; Grant number: 21590437, 24590480, 23590457

*Correspondence to: Division of Microbiology and Infectious Diseases, Department of Pathology, Shiga University of Medical Science, Setatsukinowa-cho, Otsu, Shiga 520-2192, Japan.

Received 5 June 2014; Revised 3 October 2014;
Accepted 3 November 2014

DOI 10.1002/mc.22258

Published online 24 January 2015 in Wiley Online Library (wileyonlinelibrary.com).

synthesis. Phosphorylation of S6K, S6, 4EBP1, and TSC2 proteins was also closely correlated with the enhanced viral replication in *drs*-KO MEFs. In these studies, Drs associated with stress-inducible GADD34 and formed a complex with TSC1/2, which suppresses the mTOR activity, indicating that Drs suppresses viral replication via an mTOR-dependent pathway.

Most proliferating tumor cells preferentially metabolize glucose via glycolysis, even under aerobic conditions [14–17]. This phenomenon is known as the Warburg effect and is a key metabolic hallmark of cancer cells. Recently, the associated molecular mechanisms and relationships with cancer-related genes have been intensively investigated [17–19]. For example, the tumor suppressor *p53* suppresses glycolysis by upregulating TIGAR transcription, which negatively regulates glycolysis via the activity of fructose 2,6-bisphosphatase [20]. Moreover, *p53* suppresses glucose uptake in cancer cells by inhibiting the expression of the glucose transporters Glut1 and Glut4, which are upregulated in cancer cells associated with the Warburg effect [21]. Oncogenic tyrosine kinases are known to activate pyruvate kinase M2 (PKM2) [22] and pyruvate dehydrogenase kinases (PDKs) [23], which determine whether pyruvate is converted to acetyl CoA for mitochondrial respiration or to lactate as the end product of glycolysis. The oncoprotein c-Myc regulates the transcription of metabolism regulatory factors, including LDH-A [24] and PKM2 [25], and miR23a/b [26], regulates glucose and glutamine metabolism. However, the relationship between the Warburg effect and malignant progression of cancer cells remains unclear. In the present study, we initially found that the acidification of the culture medium is accelerated in *drs*-KO MEF cells compared with wild-type (WT) MEF, suggesting that the Warburg effect-like metabolic shift, inducing enhanced glycolysis, is caused by the lack of *drs*. Subsequently, we confirmed this and demonstrated that *drs* regulates energy metabolism via LDH-B, leading to suppression of glycolysis.

MATERIALS AND METHODS

Cell Culture

Because *drs* is located in chromosome X, *drs* KO MEFs, and WT MEFs were prepared from male embryos following the mating of a *drs* heterozygous (+/−) female and wild-type (+/Y) male mice. Cells were immortalized by expressing the large T antigen of the simian virus 40 (SV40) [10]. Immunoblot and soft agar assays were performed using the human cell lines WI38, HaCaT, T24, DLD-1, and HeLa. Human 293 T embryonic kidney cells expressing the E1 gene of adenovirus type 5 and the large T antigen of SV40 were used to prepare recombinant retroviruses. All cells were cultured in Dulbecco's modified Eagle's medium (DMEM) supplemented with 10% fetal bovine serum (FBS).

Recombinant Retroviruses

The recombinant retroviral vector plasmid pCXbsr-*drs* was generated as described previously [10], and the recombinant retroviral vector plasmid pBABEpuro-K-Ras was purchased from Cell Biolabs, Inc. (San Diego, CA). Recombinant plasmids were transfected into 293 T cells with the helper plasmid pCL-ampho [27] using Lipofectamine-PLUS (Invitrogen, Carlsbad, CA) according to the manufacture's protocol. Amphotropic retroviruses in the culture medium were collected 48 h after transfection. Prior to infection, 2×10^5 cells were plated on 60 mm dishes and incubated overnight at 37°C. After treatment with 2 μg/ml polybrene for 30 min, viruses were added to the cultures and incubated for 1 h at 37°C. After seven days of incubation in the selection medium, 2 μg/ml blasticidin or 5 μg/ml puromycin was added, and drug-resistant colonies were pooled and used in assays.

Measurement of pH and Glucose, Lactate, and Pyruvate Concentrations

Cells were seeded at 5×10^5 cells/dish in 60 mm dishes and extracellular pH and concentrations of glucose and lactate in the media were determined. Cell pellets were collected; washed twice with PBS(−); and lysed in TXNE buffer containing 20 mM Tris-HCl (pH 7.4), 150 mM NaCl, 5 mM EDTA, and 1% Triton X-100; and intracellular pyruvate concentrations were determined. Glucose, lactate, and pyruvate concentrations were determined by the F-kit Glucose, Lactate, and Pyruvate assays (JK international, Tokyo, Japan), respectively. Pyruvate concentrations were normalized to cellular protein contents, which were determined using the Bradford method (Bio-Rad protein assay, Bio-Rad Laboratories, Hercules, CA) according to the manufacturer's protocol.

Metabolomic Analyses

Cells were washed twice in 5% mannitol solution, scraped off the dishes, and collected in methanol. Metabolomic analyses were performed by the Human Metabolome Technologies Inc., Yamagata, Japan. Capillary electrophoresis time-of-flight mass spectrometry (CE-TOFMS) was performed using an Agilent CE Capillary Electrophoresis System (Agilent Technologies, Waldbronn, Germany). Raw data from CE-TOFMS experiments were processed using MasterHands software [28]. Signal peaks corresponding to isotopomers, adduct ions, and other product ions of known metabolites were excluded, and all signal peaks potentially corresponding to authentic compounds were extracted, and their migration times (MT) were normalized to those of internal standards. Subsequently, peak alignments were performed according to m/z values and normalized MT values. Finally, peak areas were normalized to those of the internal standards MetSul and CSA for cations and anions, respectively. Relative area values were then

normalized to sample volumes. Annotation tables were produced from CE-ESI-TOFMS measurements of standard compounds, and were aligned with datasets that had similar m/z and normalized MT values.

Measurements of Respiratory Capacities and Glycolysis Rates

Cells were seeded at 2×10^4 cells/well in 24-well V7 XF assay plates and cultured overnight under normal culture conditions. Oxygen consumption rates (OCR), extracellular acidification rates (ECAR), and respiratory capacities of cells were then assessed by extracellular flux analyses using the XFe24 Flux analyzer and XF Cell Mito Stress Test Kit (Seahorse Bioscience, North Billerica, MA) according to the manufacturer's protocol.

Immunoblot Analysis

Cells were lysed in Laemmli sample buffer containing 62.5 mM Tris-HCl (pH 6.8), 10% glycerol, 5% 2-mercaptoethanol, 2% sodium dodecyl sulfate (SDS), and 0.01% bromophenol blue. Aliquots of cell lysates were subjected to SDS-polyacrylamide gel electrophoresis (PAGE), and separated proteins were electrotransferred onto membrane filters (Immobilon-P; Millipore, Billerica, MA). After blocking filters with TBS-T containing 10 mM Tris-HCl (pH 7.6), 150 mM sodium chloride, 0.1% Tween 20, and 5% bovine serum albumin (BSA), they were incubated overnight with the indicated primary antibodies in TBS-T with 2% BSA at 4°C. Filters were then washed in TBS-T and incubated for 1 h in horseradish peroxidase-conjugated anti-mouse or anti-rabbit IgG (GE Healthcare, Tokyo, Japan) diluted at 1:20 000 in TBS-T with 2% BSA. After several washes in TBS-T, immunoreactivity was detected using the ECL system (GE Healthcare Japan, Tokyo, Japan) according to the manufacturer's protocol.

Measurement of LDH Activity

Cells were washed twice in PBS(−) and lysed in hypotonic lysis buffer containing 20 mM HEPES (pH 7.0), 5 mM KCl, 1 mM $MgCl_2$, and 5 mM DTT supplemented with 1% protease inhibitor (Nacalai tesque, Kyoto, Japan). Cell lysates were then centrifuged at $16{,}000 \times g$ for 20 min and supernatants were assayed for the LDH enzyme using 50 mM Tris-HCl (pH 7.6) supplemented with 2 mM pyruvate and 150 mM NADH [29]. Spectrophotometric enzyme assays were performed by monitoring the conversion of NADH to NAD^+ in pyruvate utilizing reactions at 340 nm.

Reverse Transcriptase-Polymerase Chain Reaction (RT-PCR)

Total RNA was isolated from cultured cells and human tissues using the SV Total RNA Isolation System (Promega, Madison, WI). The isolated RNA was used for first-strand cDNA synthesis usingSuperscript™ III Reverse Transcriptase (Invitrogen) and an Oligo(dT) 12–18 primer (Invitrogen) for 50 min at 42°C. Conventional semi-quantitative RT-PCR was performed as previously described [13]. The sequences of the primers for RT-PCR were as follows: drs, 5′-TTAAGTGAGCTGTGCAGCCT-3′ (forward) and 5′-TAACAGCACATCAGACGTTGC-3′ (reverse); and glyceraldehyde-3-phosphate dehydrogenase (GAPDH), 5′-ACCACAGTCCATGCCATCAC-3′(forward) and 5′-TCCACCACCCTGTTGCTGTA-3′(reverse). Quantitative RT-PCR (qRT-PCR) was performed using the LightCycler 480 System with LightCycler 480 SYBR Green I master mix (Roche Diagnostics, Tokyo, Japan) in 20 μL reaction volumes containing 1 μL template cDNA (equivalent to 100 ng total RNA) and 0.5 μM of forward and reverse primers according to the manufacturer's protocol. Primer sequences for qRT-PCR were as follows [30]: LDH-A, 5′-GGACAGTGCCTACGAGGTGAT-3′ (forward) and 5′-GGATGCACCCGCCTAAGG-3′ (reverse); LDH-B, 5′-GGGAAAGTCTCTGGCTGATGAA-3′ (forward) and 5′-CTGTCACAGAGTAATCTTTATCGGC-3′ (reverse); Drs, 5′-TTAAGTGAGCTGTGCAGCCT-3′ (forward) and 5′-TAACAGCACATCAGACGTTGC-3′ (reverse); and GAPDH, 5′-GGTGAAGGTCGGTGTGAACG-3′ (forward) 5′-CTCGCTCCTGGAAGATGGTG-3′ (reverse). Amplification was performed at 95°C for 5 min, followed by 45 cycles of 95°C for 10 s, 55°C for 10 s, and 72°C for 15 s. The results were normalized to the GAPDH mRNA.

^{35}S Metabolic Labeling and Radioimmunoprecipitation

De novo protein synthesis was determined on the basis of [^{35}S]-methionine incorporation [31]. Cells were cultured for two days and newly synthesized proteins were labeled with EXPRE^{35}S^{35}S protein labeling mix™ (100 μCi/dish; Perkin Elmer, Waltham, MA) in methionine- and cysteine-free DMEM supplemented with dialyzed 10% FBS for 30 min. Treated cells were lysed in radioimmunoprecipitation assay (RIPA) buffer containing 20 mM Tris-HCl (pH 7.4), 150 mM NaCl, 5 mM EDTA, 1% Triton X-100, 1% sodium deoxycholate, 0.1% SDS, and 1% protease inhibitor cocktail (Nacalai tesque, Kyoto, Japan) and were centrifuged for 20 min at $10{,}000 \times g$ at 4°C. Supernatants were incubated with primary antibodies at 4°C for 1 h and immunocomplexes were bound to protein-G sepharose for 1 h at 4°C and washed three times with the RIPA buffer. Protein-G sepharose bound proteins were eluted by boiling in the Laemmli–SDS sample buffer for 3 min. After centrifugation at $10{,}000 \times g$ for 2 min, supernatants were subjected to SDS-PAGE. To visualize radioimmunoprecipitates, SDS-PAGE gels were fixed with 40% methanol and 10% acetic acid, dried, and exposed to X-Ray films (Fujifilm, Kanagawa, Japan).

Soft Agar Assay

Anchorage-independent growth was determined on the basis of colony-forming abilities in soft agar [3].

Briefly, cells were plated on 60 mm dishes containing 0.4% Noble agar containing DMEM supplemented with 10% FBS. After three weeks of incubation, the number of colonies >0.15 mm in diameter on each plate were counted.

Antibodies and Inhibitors

Anti-Glut4 (#2299), anti-phospho-PKM2 (Tyr105, #3827), and anti-LDH-A (#2012) rabbit polyclonal antibodies and anti-PKM2 (D78A4) and GAPDH (D16H11) rabbit monoclonal antibodies were purchased from Cell Signaling Technology (Tokyo, Japan). Anti-TIGAR (ab62533) and anti-PDK4 (ab63157) rabbit polyclonal antibodies were purchased from Abcam (Tokyo, Japan). The anti-LDH-B (EP1566Y) rabbit monoclonal antibody was purchased from Epitomics (Burlingame, CA). The anti-Glut1 (NB110–39113) rabbit polyclonal antibody was purchased from Novus Biologicals (Littleton, CO). The anti-phosphofructokinase-M (PFK; 55028-1-AP) rabbit polyclonal antibody was purchased from the ProteinTech group (Chicago, IL). The anti-Ras (clone18) mouse monoclonal antibody was purchased from BD Biosciences. Anti-α-tubulin (DM1A) and anti-Flag (M2) mouse monoclonal antibodies were purchased from Sigma (St. Luis, MO). Sodium oxamate and rapamycin were purchased from Nacalai tesque and Cell Signaling Technology, respectively.

RESULTS

Alterations of Glucose Metabolism in *drs*-Deficient Cells

To investigate the physiological roles of *drs*, we established WT and *drs*-KO MEF cell lines. No significant differences in proliferation, senescence, or morphology were observed between WT and KO cells under normal culture conditions [12] (Figure 1A). Moreover, no remarkable differences between WT and KO cells were observed during the growing phase before confluence. However, changes in the color of the culture medium indicated more rapid acidification in KO cells than in WT cells after reaching confluence (Figure 1B). The pH value of the culture medium from KO cells was significantly lower than that from WT cells after reaching confluence on day 3 (Figure 1B), indicating increased acidic end-products from KO cells. Alterations in glucose metabolism during malignant transformation of cancer cells are known as the Warburg effect, which is characterized by increased glucose transport and higher rates of glycolysis, with increased lactate production and reduced pyruvate oxidation [15,16]. To clarify whether enhanced acidification of culture medium in KO cells is due to glucose metabolism, we determined extracellular lactate and glucose concentrations and intracellular pyruvate concentrations in WT and KO cells. Extracellular lactate concentrations were significantly higher in KO cells than in WT cells on day 1, and this difference increased from days 2 to 3 (Figure 1C). Extracellular glucose concentrations in KO cells were less than those of WT cells after day 2 (Figure 1D), whereas intracellular pyruvate concentrations were similar between WT and KO cells until day 3, but they were increased in KO cells on day 4 (Figure 1E). These observations indicate that glycolysis was accelerated during culture of *drs*-KO cells.

To further investigate metabolic changes in KO cells, we performed metabolomic analyses and compared the major intracellular metabolites between WT and KO cells on days 1 and 3. Both heat map patterns (Figure 2A) and principle component analyses (Figure 2B) indicated marked differences in metabolic patterns between WT and KO cells on day 1. Moreover, metabolic patterns between WT and KO cells differed markedly between days 1 and 3 (Supplementary Figure and Supplementary table). Among 196 metabolites detected on day 1, 35 were significantly ($P < 0.05$ by Welch's t-test and $q < 0.2$ by false discovery rate method) [32] increased and eight were significantly decreased in KO cells compared with WT cells (Supplementary table). After classifying these compounds and mapping the metabolites into general biochemical pathways, as illustrated in KEGG (http://www.genome.jp/kegg/kegg2.html), the metabolic differences between WT and KO cells were attributable to the pentose phosphate pathway (PPP) and glycolysis (seven out of 43), but did not involve the TCA cycle (changes in glucose metabolite concentrations, glycolysis, PPP, and the TCA cycle are shown in Figure 2C.) Whereas glycolytic and PPP activities were increased in KO cells compared with WT cells, and those of the TCA cycle were slightly changed, suggesting that the *drs*-KO cell metabolism is dominated by glycolysis rather than respiration. To confirm metabolic shifts in KO cells, we evaluated OCR and ECAR in living cells using an Extracellular Flux Analyzer. ECAR in KO cells was significantly higher than that in WT cells, indicating increased glycolytic activity (Figure 2D). Although the total cellular OCR was similar between WT and KO cells, spare mitochondrial respiratory capacities [33] were reduced in KO cells compared with WT cells (Figure 2E). Taken together, these data demonstrate a metabolic shift with enhanced glycolysis in *drs*-KO cells.

Upregulation of LDH-B in *drs* Deficient Cells

Alterations of expression or activity of glycolysis regulatory proteins in cancer cells are closely correlated with the induction of the Warburg effect [17,19]. To investigate the mechanisms of metabolic shifts in *drs*-KO cells, we examined the expression and activation states of these glycolysis regulators using immunoblotting (Figures 3A). Expressions of Glut-1,

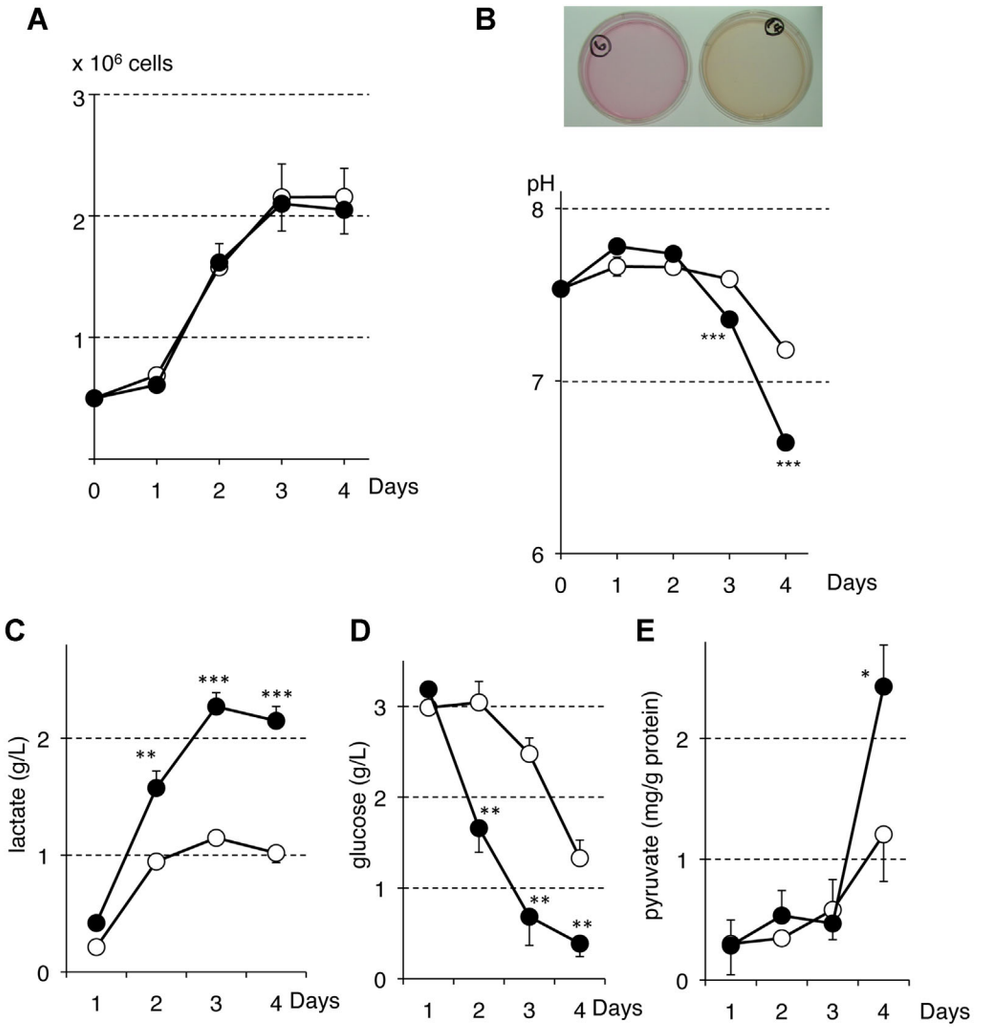

Figure 1. Comparisons of cell proliferation, extracellular pH, glucose and lactate concentrations and amount of intracellular pyruvate between wild-type (WT) and *drs*-knockout (KO) cells 5×10^5 cells were plated into 60 mm dishes on day 0 and cell numbers were counted every day. White and black circles represent WT and KO cells, respectively. Assays were performed in triplicate dishes. Error bars indicate standard deviations; $^*P < 0.05$, $^{**}P < 0.01$, and $^{***}P < 0.001$ by Welch's t-test. (A) Cell proliferation of WT and KO cells; (B) Extracellular pH of WT and KO cells; Images of the dishes on day 3 are shown. (C) Extracellular concentrations of lactate in WT and KO cells; (D) Extracellular concentration of glucose in WT and KO cells; (E) The amount of intracellular pyruvate in WT and KO cells.

Glut-4, TIGAR, and PFK-M (muscle-type) and the phosphorylation of PKM2, did not differ significantly between WT and KO cells during cultivation from days 1 to 4. In contrast, LDH-A expression in KO cells was higher than that in WT cells from days 1 to 3. Although LDH-B expression was similar in WT and KO cells on day 1, it was significantly increased from days 2 to 4 in KO cells. The expression of PDK4, which suppresses the conversion of pyruvate to acetyl-CoA, was increased in KO cells on day 4, reflecting increased intracellular pyruvate concentrations (Figure 1E). These observations suggest that enhanced expressions of LDH-A and LDH-B follow a metabolic shift in *drs*-KO cells.

LDH is a homo- or hetero-tetrameric enzyme comprising LDH-A and LDH-B subunits, which are encoded by highly related genes; it reversibly catalyzes the conversion of pyruvate to lactate [34]. Because the enzymatic activity of LDH is regulated by its expression levels and isozymic compositions [35], we examined relative enzymatic activities of LDH in WT and KO cells. The LDH activity in KO cells was slightly higher than that in WT cells on day 1, potentially reflecting a higher basal expression of LDH-A protein in KO cells (Figure 3B). This activity was significantly enhanced in KO cells compared with WT cells on days 2 to 4, reflecting the increased expression of LDH-B (Figures 3A) and higher

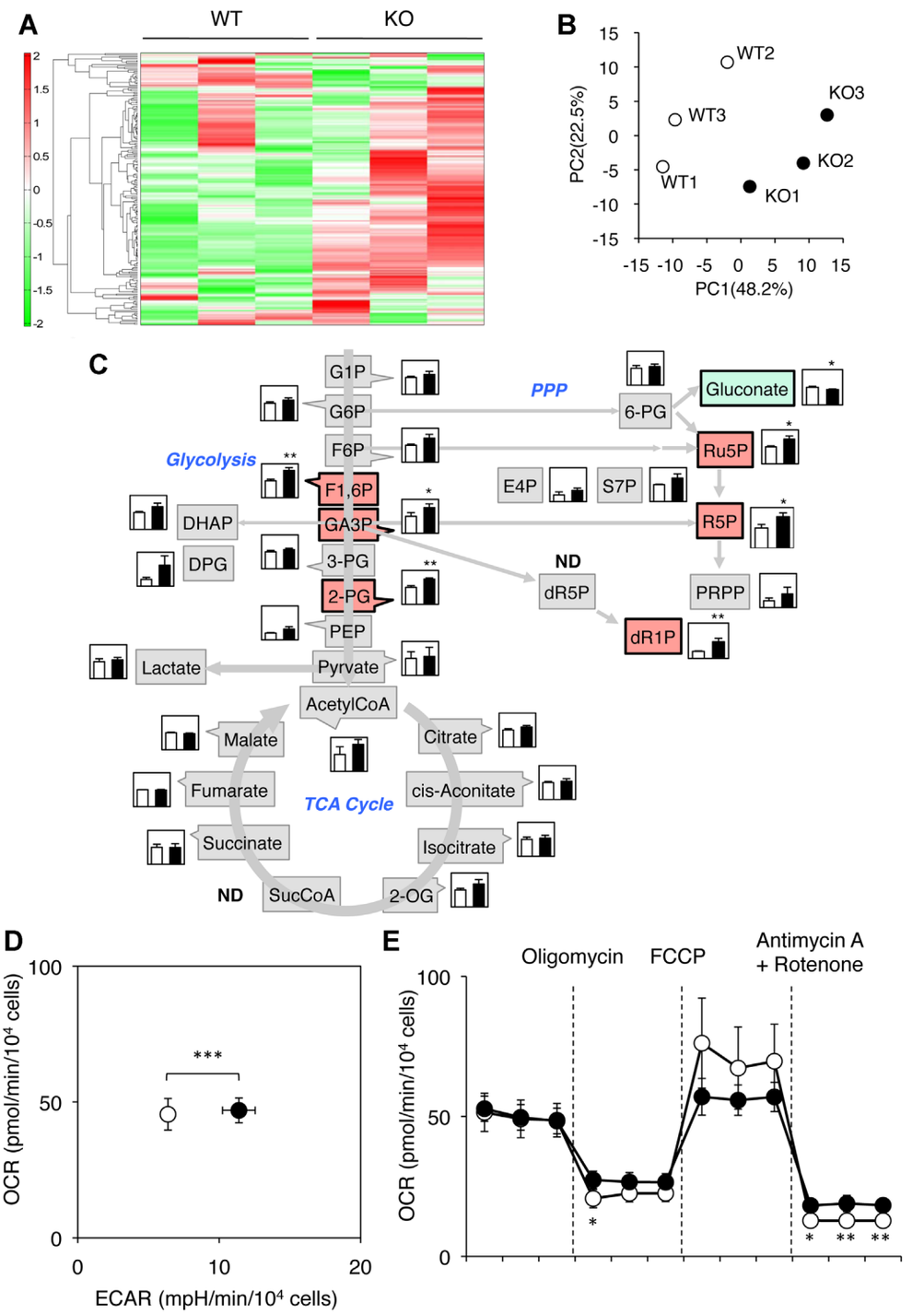

Figure 2. Metabolomic and extracellular flux analyses of wild-type (WT) and *drs*-knockout (KO) cells. (A) Hierarchical clustering and heat map representation of metabolites in WT and KO cells; Samples of WT and KO cells were collected and examined in triplicate on day 1. The color-coded scale (green, downregulation, and red, upregulation) for normalized expression values is indicated at the left. (B) Principle component analysis of metabolites in WT and KO cells; Samples of WT and KO cells were collected and examined in triplicate on day 1. White and black circles represent WT and KO cells, respectively. (C) Pathway mapping of the metabolites involved in glycolysis, the pentose phosphate pathway, and the TCA cycle; Metabolites that were significantly regulated in KO cells compared with WT cells are represented in red and green, respectively. White and black bars represent WT and KO cells, respectively. Error bars indicate means ± standard deviations of three samples; $*P < 0.05$, $**P < 0.01$ by Welch's t-test. (D) Basal oxygen consumption rates (OCR) and extracellular acidification rates (ECAR) of WT and KO cells were determined by extracellular flux analyses. White and black circles indicate WT and KO cells, respectively. Data are presented as means ± standard deviations of four samples; $***P < 0.001$ by Welch's t-test. (E) OCR determined before (basal) and after sequential injections of indicated compounds; oligomycin (1 μM), FCCP (1 μM), or antimycin A (1 μM) plus rotenone (1 μM). White and black circles indicate WT and KO cells, respectively. Data are presented as means ± standard deviations of four samples; $*P < 0.05$, $**P < 0.01$ by Welch's t-test. (D) Basal oxygen consumption rates (OCR) and extracellular acidification rates (ECAR) of WT and KO cells were determined by extracellular flux analyses. White and black circles indicate WT and KO cells, respectively. Data are presented as means ± standard deviations of four samples; *** $p < 0.001$ by Welch's t-test. (E) OCR determined before (basal) and after sequential injections of indicated compounds; oligomycin (1 μM), FCCP (1 μM), or antimycin A (1 μM) plus rotenone (1 μM). White and black circles indicate WT and KO cells, respectively. Data are presented as means ± standard deviations of four samples; * $p < 0.05$, ** $p < 0.01$ by Welch's t-test.

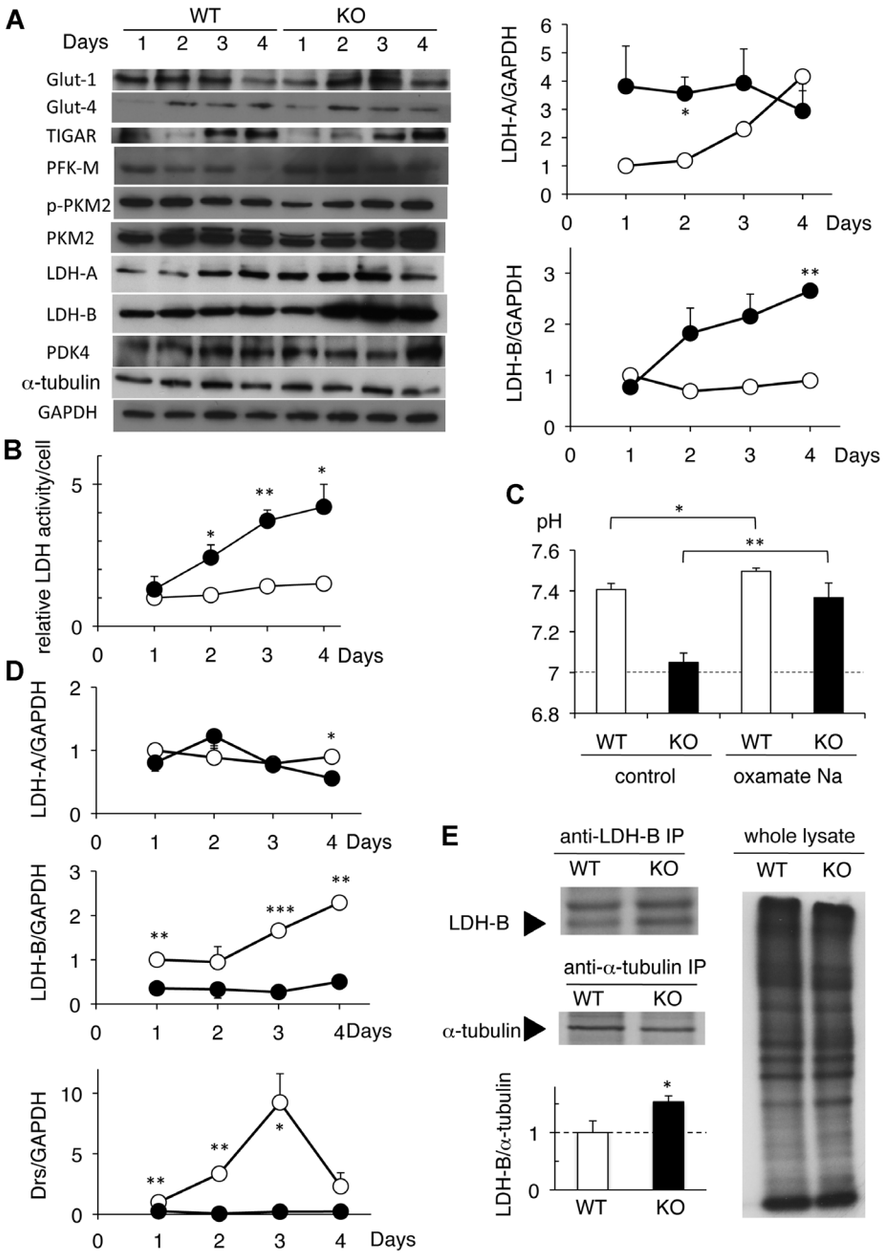

Figure 3. Changes in expression and activity of glycolysis regulatory proteins in wild-type (WT) and *drs*-knockout (KO) cells. (A) Immunoblot analyses of expression and activation of glycolysis regulatory proteins in WT and KO cells; 5×10^5 cells were plated on 60 mm dishes on day 0 and samples were collected on the indicated days. Changes in lactate dehydrogenase (LDH)-A (right-top) and LDH-B (right-bottom) protein levels in WT and KO cells were also shown. Densitometric data were normalized to glyceraldehyde-3-phosphate dehydrogenase (GAPDH) and are presented as means ± standard deviations of three independent immunoblot assays. White and black circles indicate WT and KO cells, respectively; $*P < 0.05$, $**P < 0.01$ by Welch's t-test. (B) LDH enzyme activity in WT and KO cells; Data are presented as means ± standard deviations of relative activities from triplicate samples; White and black circles indicate WT and KO cells, respectively; $*P < 0.05$, $**P < 0.01$ by Welch's t-test. (C) Extracellular pH of WT and KO cells treated with the LDH inhibitor sodium oxamate; 5×10^5 cells were plated on 60 mm dishes on day 0 and 5 mM sodium oxamate was added on day 1. Bars represent means ± standard deviations of triplicate samples on day 3. White and black bars indicate WT and KO cells, respectively; $*P < 0.05$, $**P < 0.01$ by Welch's t-test. (D) Quantitative reverse transcriptase-polymerase chain reaction analyses of LDH-A, LDH-B, and *drs* mRNA in wild-type (WT) and knockout (KO) cells; Data were normalized to the expression of GAPDH mRNA and are presented as means ± standard deviations of triplicate samples. White and black circles indicate WT and KO cells, respectively; $*P < 0.05$, $**P < 0.01$, $***P < 0.001$ by Welch's t-test. (E) *De novo* protein synthesis of LDH-B in WT and KO cells; 5×10^5 cells were plated on 60 mm dishes on day 0 and were labeled with EXPRE^{35}S^{35}S protein labeling mix for 30 min on day 2. Labeled cells were lysed in radioimmunoprecipitation assay buffer and were immunoprecipitated using antibodies for LDH-B (top-left) and α-tubulin (bottom-left), and ^{35}S incorporation was measured as described in the Materials and Methods section. Incorporation of ^{35}S of whole lysates in sodium dodecyl sulfate-polyacrylamide gel electrophoresis analysis is also presented (right). The relative amounts of synthesized LDH-B protein (LDH-B/α-tubulin) in WT and KO cells were presented as means ± standard deviations of triplicate samples; $*P < 0.05$ by Welch's t-test.

extracellular lactate concentrations (Figure 2C). These data suggest that an enhanced expression of LDH-B is responsible for the enhanced activity of LDH and increased production of lactate. Furthermore, the LDH inhibitor, sodium oxamate, inhibited decreases in pH in KO cells (Figure 3C), indicating that an enhanced LDH activity and increased LDH-B expression reflect metabolic shifts in KO cells.

To identify mechanisms of *drs* regulated LDH expression, we compared expressions of LDH-A and LDH-B mRNAs in WT and KO MEF cells using qRT-PCR (Figure 3D). The LDH-A mRNA expression was similar in WT and KO cells, whereas that of LDH-B mRNA was lower in KO cells than in WT cells, indicating that the enhanced LDH-B protein expression in KO cells is not caused by the increased LDH-B mRNA expression. After day 2, *drs* mRNA was induced in WT cells but not in KO cells. To investigate whether *drs* regulates LDH-B protein expression at the post-transcriptional level, *de novo* syntheses of the LDH-B protein was compared between WT and KO cells. Both cell types were labeled with [^{35}S]-methionine on day 2, and levels of incorporated radioactivity were compared using immunoprecipitation with a specific antibody for LDH-B. The *de novo* protein synthesis of LDH-B was significantly higher in KO cells than in WT cells, although ongoing synthesis of whole proteins and α-tubulin in KO cells were similar to that in WT cells (Figure 3E). These results indicate that *drs* regulates the *de novo* LDH-B protein synthesis.

To confirm the involvement of *drs* in LDH-related metabolic shifts, we introduced *drs* into KO cells using a retrovirus vector and investigated the extracellular acidification, respiration, LDH-B expression, and LDH activity (Figure 4). Exogenous expressions of *drs* mRNA and Drs protein were confirmed by RT-PCR and immunoblot analysis with anti-Flag antibody (Figure 4A). We found that *drs* suppressed the extracellular acidification (Figures 4B and C) and enhanced mitochondrial respiration (Figure 4D), as well as the induction of LDH-B protein expression (Figure 4E) and LDH activity (Figure 4F) in KO cells. Taken together, these results indicate that the absence of *drs* leads to an enhancement of LDH-B expression, increased LDH activity, and a metabolic shift leading to enhanced glycolysis.

Correlation Between *drs* Downregulation and LDH-B Expression in Transformed Cells

To investigate the correlation between enhanced LDH-B expression and *drs* downregulation in transformed cells, we introduced activated *K-ras* into WT MEF cells using a retrovirus vector. Previously, we showed that transformation with oncogenes downregulates endogenous *drs* expression [1]. Similarly, in this study, the introduction of activated *K-ras* suppressed the expression of *drs* mRNA in WT cells (Figure 5A). The expression of LDH-B protein was increased in WT MEF cells expressing activated *K-ras*, suggesting that downregulation of *drs* mRNA is correlated with enhanced expression of LDH-B protein in *K-ras*-transformed MEF cells (Figure 5B). Anchorage-independent growth of *K-ras* expressing WT cells was significantly suppressed by the LDH inhibitor sodium oxamate (Figure 5C), suggesting that enhanced expression of LDH-B is involved in the regulation of transformed phenotypes following activation of *K-ras*. Furthermore, we investigated LDH-B expression in the human cancer cell lines T24, DLD-1, and HeLa, in which *drs* mRNA expression is reportedly downregulated [3]. The expression of LDH-B in these human cancer cell lines was higher than that in the human noncancer cell lines WI38 and HaCaT (Figure 5D). Treatments with sodium oxamate also partially suppressed anchorage-independent growth of DLD-1 and HeLa cells (Figure 5E). Anchorage-independent growth was undetectable in T24 cells. We also investigated the correlation between downregulation of *drs* and enhanced expression of LDH-B in human cancer tissues by online database analyses using GEO datasets (http://www.ncbi.nlm.nih.gov/gds). By searching from datasets including both cancer and normal tissues, we found significant inverse correlations between the expression levels of *SRPX* (human *drs* gene) and those of *LDHB* in human microsatellite-unstable colorectal cancer [36] (Pearson's $r = -0.350$, $P = 0.0138$) and lung adenocarcinoma [37] (Pearson's $r = -0.231$, $P = 0.0166$) tissues (Figures 5F and G). Taken together, these results suggest that down-regulation of *drs* during transformation and carcinogenesis contributes to enhanced expression of LDH-B, and it is partially involved in the expression of transformed phenotypes.

DISCUSSION

In the present study, we used *drs*-KO MEFs to demonstrate that *drs* is involved in the regulation of glucose metabolism via LDH-B. Extracellular acidification, lactate concentrations, and glucose consumptions in *drs*-KO cells increased significantly and more rapidly than those in WT cells. Metabolomic and extracellular flux analyses also confirmed enhanced glycolysis in *drs*-KO cells. In particular, LDH-B was upregulated in a post-transcriptional manner and LDH activity was increased in *drs*-KO cells. Increased LDH-B expression, LDH activity, and acidification of culture medium in *drs*-KO MEFs were suppressed by retroviral gene rescue of *drs*, indicating that the present Warburg effect-like metabolic shift via LDH-B is due to the lack of *drs*. These results indicate that LDH-B plays a critical role for the regulation of glycolysis by *drs*.

Recent studies have shown that the expression of LDH-B is increased in certain types of cancers, including breast cancer [38,39], lung adenocarcinomas [40], maxillary sinus squamous cell carcinomas [41], and

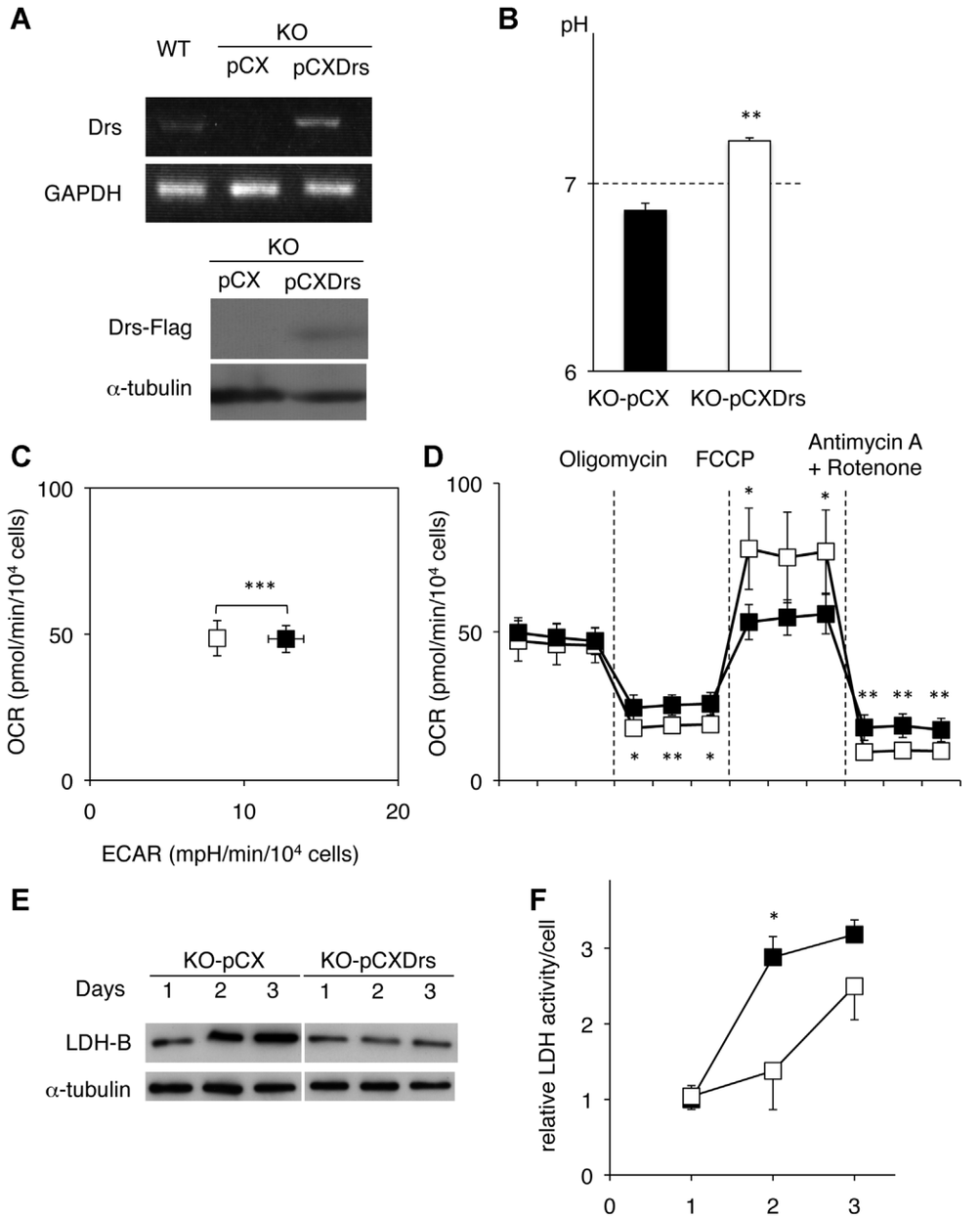

Figure 4. Effects of virally introduced *drs* in knockout (KO) cells. (A) Reverse transcriptase-polymerase chain reaction analyses of endogenous and introduced *drs* mRNA in WT and KO cells; glyceraldehyde-3-phosphate dehydrogenase (GAPDH) mRNA expression was used as an internal control. Immunoblot analysis of exogenous Drs protein tagged with Flag in KO cells was also shown; α-tubulin protein expression was used as an internal control. Anti-Flag antibody was used to detect exogenous Drs-Flag protein. (B) Extracellular pH in vector virus (KO-pCX) or *drs* expressing virus (KO-pCXDrs) transfected *drs* KO cells; 5×10^5 cells were plated on 60 mm dishes on day 0 and extracellular pH was measured on day 3. Bars indicate means ± standard deviations of triplicate samples. Black and white bars indicate KO-pCX and KO-pCXDrs, respectively; $^{**}P < 0.01$ by Welch's t-test. (C) Basal oxygen consumption rates (OCR) and extracellular acidification rates (ECAR) in KO-pCX and KO-pCXDrs cells were determined by extracellular flux analyses; Black and white squares indicate KO-pCX and KO-pCXDrs cells, respectively. Data are presented as means ± standard deviations of four samples; $^{***}P < 0.001$ by Welch's t-test. (D) OCR determined before (basal) and after sequential injections of the indicated compounds; oligomycin (1 μM), FCCP (1 μM), or antimycin A (1 μM) plus rotenone (1 μM). Black and white squares indicate KO-pCX and KO-pCXDrs cells, respectively. Data are presented as means ± standard deviations of four samples; $^{*}P < 0.05$, $^{**}P < 0.01$ by Welch's t-test. (E) Immunoblot analysis of lactate dehydrogenase (LDH)-B protein expression in KO-pCX and KO-pCXDrs cells; α-tubulin protein expression was used as an internal control. (F) LDH enzyme activity in KO-pCX and KO-pCXDrs cells. Relative activity data are presented as means ± standard deviations of triplicate samples. Black and white squares indicate KO-pCX and KO-pCXDrs cells, respectively; $^{*}P < 0.05$ by Welch's t-test.

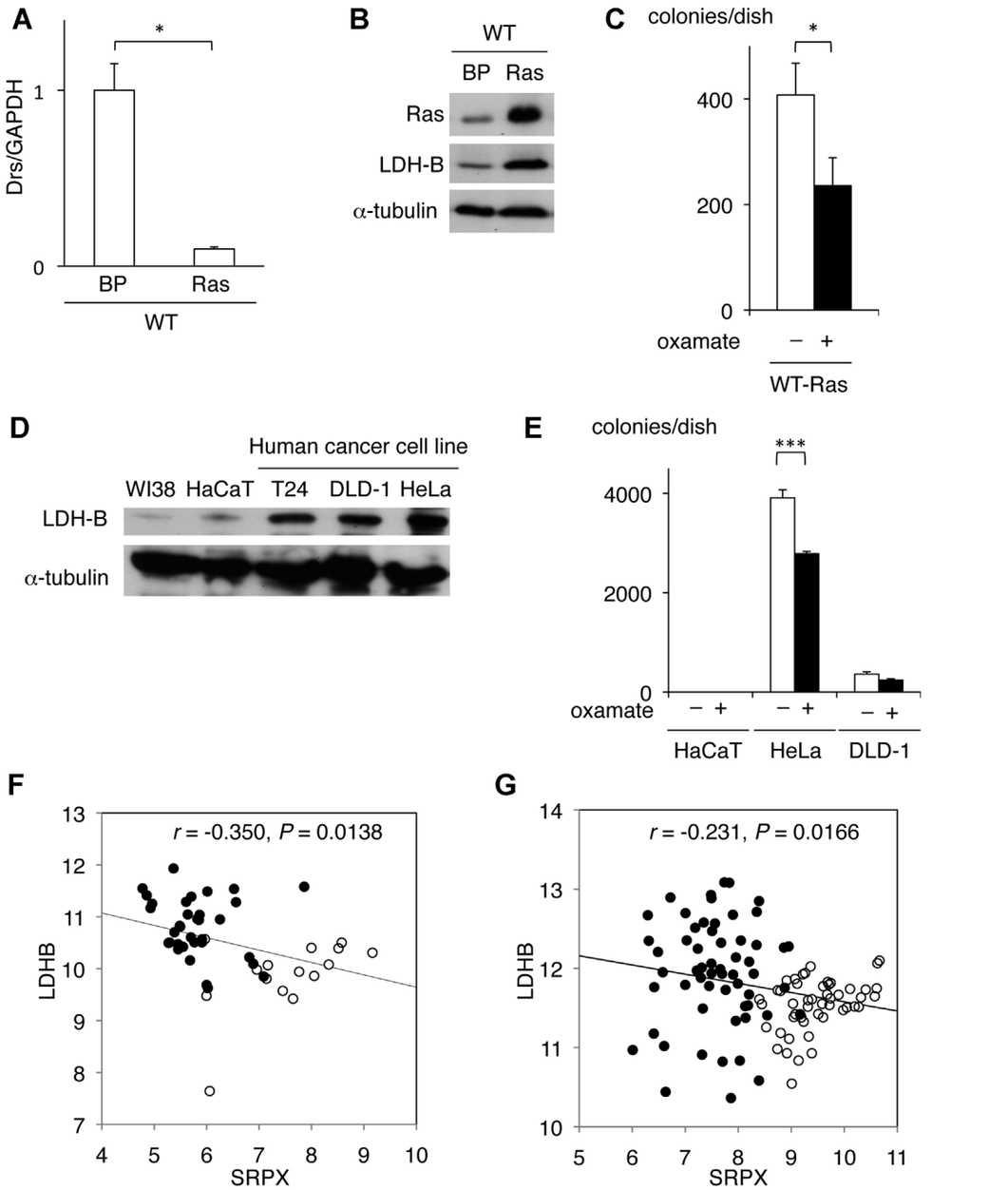

Figure 5. The effect of activated *K-ras* on the expression of *drs* and lactate dehydrogenase (LDH)-B. (A) Quantitative reverse transcriptase-polymerase chain reaction analysis of *drs* mRNA in wild-type (WT) cells after retroviral introduction of activated *K-ras*; Data were normalized to the expression of glyceraldehyde-3-phosphate dehydrogenase (GAPDH) mRNA and are presented as means ± standard deviations of triplicate samples; $*P < 0.05$ by Welch's *t*-test. (B) Immunoblot analyses of introduced activated *K-Ras* in WT cells; α-tubulin expression was used as an internal control. (C) The effect of an LDH inhibitor on colony forming abilities of WT cells expressing activated *K-ras* in soft agar; Black and white bars indicate numbers of colonies in soft agar in the presence and absence of 5 mM sodium oxamate, respectively. Bars represent means ± standard deviations of triplicate samples; $*P < 0.05$ by Welch's *t*-test. (D) Expression of LDH-B proteins in human cell lines; α-tubulin expression was used as an internal control. (E) The effect of an LDH inhibitor on colony forming abilities of HaCaT, HeLa, and DLD-1 cells in soft agar; Black and white bars represent cells incubated in the presence and absence of 5 mM sodium oxamate, respectively. Bars represent means ± standard deviations of triplicate samples; $***P < 0.001$ by Welch's *t*-test. (F and G) Correlations between *SRPX* (human *drs*) and *LDHB* expression in human colorectal and lung cancers; The gene expression profiles in normal and cancer tissues were obtained from GEO datasets for microsatellite-unstable colorectal cancers (F, GDS4515; 34 normal and 15 cancer tissues), and lung adenocarcinomas (G, GDS3257; 49 normal and 58 tumor tissues). Black and white circles represent individual tumor and normal tissues, respectively. Values indicate Pearson's correlation coefficient (*r*) with *P*-value.

thyroid tumors [42]. Zha et al. showed that LDH-B is a downstream target of mTOR that is critical for hyperactive mTOR-mediated tumorigenesis [30]. We previously reported that Drs suppresses the mTOR pathway by binding to stress-inducible GADD34 and TSC1/2 proteins, which are upstream regulators of mTOR [13], suggesting a correlation between LDH-B expression and mTOR activity. In breast cancer cells, activation of mTOR led to an increased LDH-B expression via STAT3 [30]. However, the de novo protein synthesis of LDH-B was upregulated in *drs*-KO MEF cells independent of STAT3 phosphorylation (data not shown). Although mTOR and LDH-B may play critical roles in the regulation of glucose metabolism by *drs*, further investigations are required to elucidate the associated molecular mechanisms.

We also investigated the relationship between regulation of glucose metabolism by *drs* and transformation. In activated *K-ras*-transformed WT MEF cells, expression of endogenous *drs* mRNA was markedly suppressed, whereas LDH-B expression was increased (Figure 5). LDH-B expression was also increased in human cancer cell lines with low *drs* expression. Furthermore, the LDH inhibitor sodium oxamate suppressed anchorage-independent growth in activated *K-ras* transformed MEF cells; however, this suppression was less marked in human cancer cell lines. These data suggest that downregulation of *drs* may contribute to the Warburg effect, which is closely associated with malignant progression of cancer cells. We also found from online database analyses that downregulation of *drs* is correlated with enhanced expression of *LDHB* in human colorectal cancer and lung adenocarcinoma tissues (Figures 5F and G), supporting this idea. The expression of *drs* mRNA was downregulated in a variety of human malignant cancers, including colon cancers, lung adenocarcinomas, and prostate carcinomas [4,5,7]. *K-ras* mutations have been frequently reported in human colorectal and lung cancers [43,44]. Although the genetic loss of *drs* hardly conferred transformed phenotypes in normal MEF cells, it significantly increased sensitivity to transformation by v-*src* and activated *K-ras* [[10] and unpublished data]. Activated *K-ras* suppressed the expression of *drs* mRNA (Figure 5B), and it was associated with the increased expression of LDH-B (Figure 5A). These results suggest that the downregulation of *drs* by *K-ras* contributes to the upregulation of LDH-B, although we cannot completely exclude the possibility that, in addition to *drs*, *K-ras* is also directly involved in the upregulation of LDH-B. The retroviral oncogenes v-*src*, v-*fps*, and v-*abl* suppressed endogenous *drs* expression [1]. Some oncogenes have been shown to be involved in the induction of the Warburg effect [17,19]. Thus, downregulation of *drs* by oncogenes or other mechanisms may lead to induction of the Warburg effect in cancer cells. Finally, anchorage-independent growth was suppressed by LDH inhibitor sodium oxamate in both transformed MEF cells and human cancer cells, suggesting that inhibition of enhanced glycolysis suppresses transformed phenotypes. Thus, therapeutic applications of LDH inhibitors and other agents that suppress glycolysis may be useful for the treatment of malignant cancers.

ACKNOWLEDGMENTS

We would like to thank Akiyo Ushio (Shiga University of Medical Science) for the technical assistance. This project is supported by Grants-in-Aids for Scientific Research from the Japan Society for the Promotion of Science (JSPS KAKENHI; Grant numbers 21590437, 24590480, and 23590457).

REFERENCES

1. Pan J, Nakanishi K, Yutsudo M, et al. Isolation of a novel gene down-regulated by v-src. FEBS Lett 1996;383: 21–25.
2. Inoue H, Pan J, Hakura A. Suppression of v-src transformation by the drs gene. J Virol 1998;72:2532–2537.
3. Yamashita A, Hakura A, Inoue H. Suppression of anchorage-independent growth of human cancer cell lines by the drs gene. Oncogene 1999;18:4777–4787.
4. Shimakage M, Kawahara K, Kikkawa N, Sasagawa T, Yutsudo M, Inoue H. Down-regulation of drs mRNA in human colon adenocarcinomas. Int J Cancer 2000;87:5–11.
5. Shimakage M, Takami K, Kodama K, Mano M, Yutsudo M, Inoue H. Expression of drs mRNA in human lung adenocarcinomas. Hum Pathol 2002;33:615–619.
6. Mukaisho K, Suo M, Shimakage M, Kushima R, Inoue H, Hattori T. Down-regulation of drs mRNA in colorectal neoplasms. Jpn J Cancer Res 2002;93:888–893.
7. Kim CJ, Shimakage M, Kushima R, et al. Down-regulation of drs mRNA in human prostate carcinomas. Hum Pathol 2003;34:654–657.
8. Shimakage M, Inoue N, Ohshima K, et al. Downregulation of drs mRNA expression is associated with the progression of adult T-cell leukemia/lymphoma. Int J Oncol 2007; 30:1343–1348.
9. Shimakage M, Kodama K, Kawahara K, et al. Downregulation of drs tumor suppressor gene in highly malignant human pulmonary neuroendocrine tumors. Oncol Rep 2009;21: 1367–1372.
10. Tambe Y, Yoshioka-Yamashita A, Mukaisho K, et al. Tumor prone phenotype of mice deficient in a novel apoptosis-inducing gene, drs. Carcinogenesis 2007;28:777–784.
11. Tambe Y, Isono T, Haraguchi S, Yoshioka-Yamashita A, Yutsudo M, Inoue H. A novel apoptotic pathway induced by the drs tumor suppressor gene. Oncogene 2004;23: 2977–2987.
12. Tambe Y, Yamamoto A, Isono T, Chano T, Fukuda M, Inoue H. The drs tumor suppressor is involved in the maturation process of autophagy induced by low serum. Cancer Lett 2009;283:74–83.
13. Tambe Y, Okuyama N, Nakagawa T, et al. Suppression of viral replication by drs tumor suppressor via mTOR dependent pathway. Cancer Lett 2012;314:82–91.
14. Warburg O. On the origin of cancer cells. Science 1956;123: 309–314.
15. Hsu PP, Sabatini DM. Cancer cell metabolism: Warburg and beyond. Cell 2008;134:703–707.

16. Vander Heiden MG, Cantley LC, Thompson CB. Understanding the Warburg effect: the metabolic requirements of cell proliferation. Science 2009;324:1029–1033.
17. Cairns RA, Harris IS, Mak TW. Regulation of cancer cell metabolism. Nat Rev Cancer 2011;11:85–95.
18. Levine AJ, Puzio-Kuter AM. The control of the metabolic switch in cancers by oncogenes and tumor suppressor genes. Science 2010;330:1340–1344.
19. Dang CV. Links between metabolism and cancer. Genes Dev 2012;26:877–890.
20. Bensaad K, Tsuruta A, Selak MA, et al. TIGAR, a p53-inducible regulator of glycolysis and apoptosis. Cell 2006;126:107–120.
21. Schwartzenberg-Bar-Yoseph F, Armoni M, Karnieli E. The tumor suppressor p53 down-regulates glucose transporters GLUT1 and GLUT4 gene expression. Cancer Res 2004;64: 2627–2633.
22. Dang CV. PKM2 tyrosine phosphorylation and glutamine metabolism signal a different view of the Warburg effect. Sci Signal 2009;2:pe75.
23. Schulze A, Downward J. Flicking the Warburg switch-tyrosine phosphorylation of pyruvate dehydrogenase kinase regulates mitochondrial activity in cancer cells. Mol Cell 2011;44:846–848.
24. Shim H, Dolde C, Lewis BC, et al. C-Myc transactivation of LDH-A: Implications for tumor metabolism and growth. Proc Natl Acad Sci U S A 1997;94:6658–6663.
25. Sun Q, Chen X, Ma J, et al. Mammalian target of rapamycin up-regulation of pyruvate kinase isoenzyme type M2 is critical for aerobic glycolysis and tumor growth. Proc Natl Acad Sci U S A 2011;108:4129–4134.
26. Gao P, Tchernyshyov I, Chang TC, et al. C-Myc suppression of miR–23a/b enhances mitochondrial glutaminase expression and glutamine metabolism. Nature 2009;458:762–765.
27. Naviaux RK, Costanzi E, Haas M, Verma IM. The pCL vector system: rapid production of helper-free, high-titer, recombinant retroviruses. J Virol 1996;70:5701–5705.
28. Sugimoto M, Hirayama A, Robert M, Abe S, Soga T, Tomita M. Prediction of metabolite identity from accurate mass, migration time prediction and isotopic pattern information in CE-TOFMS data. Electrophoresis 2010;31: 2311–2318.
29. Pathak C, Jaiswal YK, Vinayak M. Modulation in the activity of lactate dehydrogenase and level of c-Myc and c-Fos by modified base queuine in cancer. Cancer Biol Ther 2008;7: 85–91.
30. Zha X, Wang F, Wang Y, et al. Lactate dehydrogenase B is critical for hyperactive mTOR-mediated tumorigenesis. Cancer Res 2011;71:13–18.
31. Minami K, Tambe Y, Watanabe R, et al. Suppression of viral replication by stress-inducible GADD34 protein via the mammalian serine/threonine protein kinase mTOR pathway. J Virol 2007;81:11106–11115.
32. Chen M, Zhou K, Chen X, et al. Metabolomic analysis reveals metabolic changes caused by bisphenol A in rats. Toxicol Sci 2014;138:256–267.
33. Brand MD, Nicholls DG. Assessing mitochondrial dysfunction in cells. Biochem J 2011;435:297–312.
34. Li SS. Human and mouse lactate dehydrogenase genes A (muscle), B (heart), and C (testis): Protein structure, genomic organization, regulation of expression, and molecular evolution. Prog Clin Biol Res 1990;344:75–99.
35. Pelicano H, Martin DS, Xu RH, Huang P. Glycolysis inhibition for anticancer treatment. Oncogene 2006;25: 4633–4646.
36. Alhopuro P, Sammalkorpi H, Niittymaeki I, et al. Candidate driver genes in microsatellite-unstable colorectal cancer. Int J Cancer 2012;130:1558–1566.
37. Landi MT, Dracheva T, Rotunno M, et al. Gene expression signature of cigarette smoking and its role in lung adenocarcinoma development and survival. PLoS One 2008;3:e1651.
38. McCleland ML, Adler AS, Shang Y, et al. An integrated genomic screen identifies LDHB as an essential gene for triple-negative breast cancer. Cancer Res 2012;72:5812–5823.
39. Dennison JB, Molina JR, Mitra S, et al. Lactate dehydrogenase B: A metabolic marker of response to neoadjuvant chemotherapy in breast cancer. Clin Cancer Res 2013;19: 3703–3713.
40. McCleland ML, Adler AS, Deming L, et al. Lactate dehydrogenase B is required for the growth of KRAS-dependent lung adenocarcinomas. Clin Cancer Res 2013;19:773–784.
41. Kinoshita T, Nohata N, Yoshino H, et al. Tumor suppressive microRNA–375 regulates lactate dehydrogenase B in maxillary sinus squamous cell carcinoma. Int J Oncol 2012; 40:185–193.
42. Mirebeau-Prunier D, Le Pennec S, Jacques C, et al. Estrogen-related receptor alpha modulates lactate dehydrogenase activity in thyroid tumors. PLoS One 2013;8:e58683.
43. Pylayeva-Gupta Y, Grabocka E, Bar-Sagi D. RAS oncogenes: weaving a tumorigenic web. Nat Rev Cancer 2011;1 1:761–774.
44. Fernández-Medarde A, Santos E. Ras in cancer and developmental diseases. Genes Cancer 2011;2:344–358.

SUPPORTING INFORMATION

Additional supporting information may be found in the online version of this article at the publisher's web-site.